^{2}H NMR Study of Dynamics, Ordering, and Phase Transitions in Ferroelectric Pyridinium Tetrafluoroborate

Bettina Beck, Jorge A.Villanueva-Garibay, Klaus Müller,* and Emil Roduner*

Universität Stuttgart, Institut für Physikalische Chemie, Pfaffenwaldring 55, D-70569 Stuttgart

Received June 3, 2002. Revised Manuscript Received February 3, 2003

Dynamic ^{2}H NMR spectroscopy employing line shape studies and spin−lattice relaxation experiments is used to investigate the molecular dynamics of the perdeuterated pyridinium cations in pyridinium tetrafluoroborate in the temperature range between 120 and 290 K. Special interest lies in the two solid−solid phase transitions occurring at 204 K and at 238.7 K. The experimental spectra show that the pyridinium cations perform fast rotation around the pseudo *C*6 axis at high temperatures. Decreasing the temperature leads to successive slowing down of the rotational motion resulting in nearly completely immobile and preferentially oriented pyridinium cations at 120 K. Simulating the spectra with a 3-site or a 6-site jump model shows that both are appropriate to describe the experimental NMR data. The models yield population probabilities which permit the calculation of the orientational contribution to the polarization and the enthalpy change. For both models distinct deviations from the macroscopic properties are found. We therefore suggest that, in addition to the cation orientation, the classical ferroelectric mechanism operates which has a partly compensating effect. A displacement of anion vs cation sublattice by 0.23−0.25 Å is sufficient to account for the missing polarization contribution. Both these ferroelectric mechanisms are potentially continuous in their onset, which is compatible with second-order transitions, but it appears that they may both be borderline cases between second and first order.

1. Introduction

An interesting family of pyridinium compounds is easily formed by a reaction of pyridine, a strong organic base, with many acids. The majority of these salts undergo a single structural solid−solid phase transition of the order−disorder type changing the cation dynamics.[1−5] In the high-temperature phase the pyridinium cation is assumed to perform fast rotation around the pseudo *C*6 axis perpendicular to the molecular plane between equivalent potential wells, whereas in the low-temperature phase the rotation should take place between inequivalent potentials. Only some of the compounds show a sequence of two transitions. The additional transition always takes place at higher temperatures and is ferroelectric.[6−10] With reference to Czarnecki et al., the very outstanding example of this family is pyridinium tetrafluoroborate ($PyBF_4$), as it is the only multiaxial ferroelectric undergoing a continuous phase transition. On cooling, the crystal transforms from $R\bar{3}m$ to *C*2 symmetry at 238.7 K, and at 204 K transforms to the space group *P*2. The transition at higher temperature is paraelectric−ferroelectric and of second order according to Czarnecki et al.[11,12] In clear contrast, Hanaya et al. are convinced that this transition must be of first order due to a different interpretation of the characteristics of the heat capacity anomalies.[13] The cation and anion structures and the unit cell are shown in Figure 1.

Up to now there is only a limited understanding of the factors which drive phase transitions or determine the order. It is well-known that ferroelectricity can be obtained via a displacement of the different ionic sublattices against each other, i.e., the classical ferroelectric mechanism; but it can also be caused by an increase in ordering of electrical dipole moments. How-

* To whom correspondence should be addressed. Tel: ++49 711 685 4490. Fax: ++49 711 685 4495. E-mail: e.roduner@ipc.uni-stuttgart.de.

(1) Wasicki, J. W.; Nawrocik, W.; Pajak, Z.; Nataniec, I.; Belushkin, A. V. *Phys. Status Solidi A* **1989**, *114*, 497.
(2) Ripmeester, J. A. *J. Chem. Phys.* **1986**, *85* (2), 747.
(3) Ripmeester, J. A. *Can. J. Chem.* **1976**, *54*, 3453.
(4) Wasicki, J.; Kozak, A.; Pajak, Z.; Czarnecki, P.; Belushkin, A. V.; Adams, M. A. *J. Chem. Phys.* **1996**, *105*, 9470.
(5) Kozak, A.; Wasicki, J.; Pajak, Z. *Phase Trans.* **1996**, *57*, 153.
(6) Czarnecki, P.; Nawrocik, W.; Pajak, Z.; Wasicki, J. *J. Phys.: Condens. Matter* **1994**, *6*, 4955.
(7) Czarnecki, P.; Maluszynska, H. *J. Phys.: Condens. Matter* **2000**, *12*, 1.
(8) Wasicki, J.; Czarnecki, P.; Pajak, Z.; Nawrocik, W.; Szczepanski, W. *J. Chem. Phys.* **1997**, *107*, 576.
(9) Pajak, Z.; Czarnecki, P.; Wasicki, J.; Nawrocik, W. *J. Chem. Phys.* **1998**, *109*, 6420.
(10) Pajak, Z.; Czarnecki, P.; Maluszynska, H.; Szafranska, B.; Szafran, M. *J. Chem. Phys.* **2000**, *113* (2), 848.
(11) Czarnecki, P.; Katrusiak, A.; Szafraniak, I.; Wasicki, J. *Phys. Rev. B* **1998**, *57* (6), 3326.
(12) Czarnecki, P.; Nawrocik, W.; Pajak, Z.; Wasicki, J. *Phys. Rev. B* **1994**, *49*, 1511.
(13) Hanaya, M.; Shibazaki, H.; Oguni, M.; Nemoto, T.; Ohashi, Y. *J. Phys. Chem. Solids* **2000**, *61*, 651.

10.1021/cm021224e CCC: $25.00
Published on Web 03/22/2003

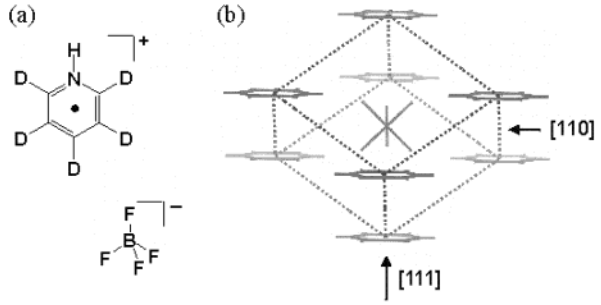

Figure 1. (a) Anion and cation structures of $PyBF_4$-d_5. (b) Schematic unit cell of $PyBF_4$ in the high-temperature phase. The structural changes at the phase transitions are minute.

ever, to describe and understand ferroelectric phase transitions, detailed information about the ionic dynamics and the time scale of the dynamics are necessary. Furthermore, the correlation between ferroelectric polarization and dynamics, as well as the effect of steric conditions on these dynamics, are of interest to understand the different behaviors of the various pyridinium compounds.

Dynamic NMR techniques have been extensively used to investigate dynamic processes in molecular solids.[14−19] ^{2}H NMR methods have demonstrated a particular suitability in evaluations of the motional and the structural characteristics on a molecular level.[19−22] Quite different chemical systems, such as inclusion compounds, liquid crystals, biological membranes, or polymers, have been studied by this means in recent years. Covering several orders of magnitude, various experimental techniques such as line shape analysis and spin−lattice relaxation measurements have been applied to study molecular processes depending on the dynamic range. The corresponding ^{2}H NMR spectra are sensitive to molecular processes with rate constants on the order of the quadrupolar coupling constant, i.e., between 10^4 and 10^8 s^{-1}. Very fast motions with rate constants between 10^8 and 10^{11} s^{-1} can be studied by spin−lattice relaxation measurements.[23] The particular situation in ^{2}H NMR spectroscopy arises from the fact that the spin Hamiltonian is dominated by the quadrupolar interaction with the main interaction axis along the C−^{2}H bond. Consequently, detailed information about actual molecular characteristics of the system under investigation can be provided by the analysis of such ^{2}H NMR experiments.

In this study we present solid-state ^{2}H NMR investigations on perdeuterated pyridinium tetrafluoroborate in the temperature range between 120 and 290 K. Special interest lies in the molecular behavior of the cation molecule in the vicinity of the two solid−solid phase transitions and in the low-temperature phase, as the characterization of $PyBF_4$ in the latter is still fragmentary. The quantitative analysis of the line shape and relaxation experiments provides a detailed insight into the cation dynamics as a function of temperature comprising three different solid phases. Moreover, the analysis leads to kinetic and thermodynamic information. As these data relate only to the cation, comparison with experimental results for the macroscopic properties from differential thermal analysis[12] or measurements of permittivity, pyroelectric effect (pyroeffect), and spontaneous polarization[11] leads to detailed information about the individual ionic contribution. Thus, it is possible to determine the intermolecular interactions which lead to ferroelectricity. Moreover the fraction of ferroelectricity caused by the classical mechanism and the contribution caused by the onset of ordering of the ions can be distinguished.

2. Experimental Section

Materials. Pyridine-d_5 (99 atom % D) and tetrafluoroboric acid (48 wt % solution in water) were purchased from Aldrich Chemicals and used without further purification. Pyridine-d_5 was added to the tetrafluoroboric acid solution at room temperature under stirring. Crystals were formed immediately and measured after drying without further purification.

NMR Studies. All ^{2}H NMR experiments were recorded on a Bruker CXP 300 spectrometer at 46.07 MHz interfaced to a Tecmag spectrometer control system. The temperature-dependent ^{2}H NMR spectra were obtained using the quadrupole echo sequence $(^{\pi}/_2)_x - \tau_1 - (^{\pi}/_2)_y - \tau_2$ with $^{\pi}/_2$ pulses of 2.2 μs and a pulse spacing of $\tau_1 = \tau_2 = 20$ μs. A modified inversion recovery sequence $(\pi - \tau_r - (^{\pi}/_2)_x - \tau_1 - (^{\pi}/_2)_y - \tau_2$ was used to determine spin−lattice relaxation times (T_{1Z}), using the quadrupole echo sequence for signal detection and varying the relaxation delay τ_r. Instead of the inversion π pulse a composite pulse was used in these experiments which is given by $(^{\pi}/_2)_{\phi}(^{\pi}/_2)_{(\phi\pm\pi/2)}(^{\pi}/_2)_{\phi}$ with phase cycling ($\phi = 0$, $^{\pi}/_2$, π, $^{3\pi}/_2$).[24] Recycle delays took at least 10 times the spin−lattice relaxation time T_{1Z}. The number of scans was 16 or 32. The sample temperature was controlled with a Bruker BVT 1000 control unit, and in general it was stable to within 1 K.

NMR Data Processing and Simulations. Experimental spin−lattice relaxation times T_{1Z} (powder values) were determined by analyzing the amplitudes of the experimental free induction decay (FID) from the inversion recovery experiments. The behavior of an $I = 1$ spin system during quadrupole echo and inversion recovery experiments was described theoretically with the help of appropriate FORTRAN programs.[25] The simulation programs are very general and account for various types of molecular motions. A numerical diagonalization of the corresponding relaxation matrixes using standard software packages gives the theoretical line shapes and relaxation times.[26] Data processing and simulation of the experiments were done on SUN workstations and personal computers using the NMR1 and Sybyl/Triad software packages (Tripos, St. Louis, MO).

In this study two different simulation models were used in order to account for the in-plane motion of the perdeuterated pyridinium cations. The simplest possible is a 3-site jump model (120° jumps) which is compatible with the symmetry of the high-temperature phase. In addition the experimental spectra were simulated with a 6-site jump model (60° jumps)

(14) Griffin, R. G. *Methods Enzymol.* **1981**, *72*, 108.
(15) Davis, J. H. *Biochim. Biophys. Acta* **1983**, *737*, 117.
(16) Spiess, H. W. *Adv. Polym. Sci.* **1985**, *66*, 23.
(17) Müller, K.; Meier, P.; Kothe, G. *Prog. Nucl. Magn. Reson. Spectrosc.* **1985**, *17*, 211.
(18) Vold, R. R.; Vold, R. L. *Adv. Magn. Opt. Res.* **1991**, *16*, 85.
(19) Ripmeester, J. In *Inclusion Compounds*; Atwood, J. L., Davies, J. E. D., MacNicol, D. D., Eds.; Oxford University Press: New York, 1991; vol. 5, p 37.
(20) Greenfield, M. S.; Vold, R. L.; Vold, R. R. *Mol. Phys.* **1989**, *66*, 269.
(21) Meirovitch, E.; Krant, T.; Vega, S. *J. Phys. Chem.* **1983**, *87*, 1390.
(22) Poupko, R.; Furman, E.; Müller, K.; Luz, Z. *J. Chem. Phys.* **1991**, *95*, 407.
(23) Torchia, D. A.; Szabo, A. *J. Magn. Res.* **1982**, *49*, 107.
(24) Heaton, N. J.; Vold, R. R.; Vold, R. L. *J. Magn. Res.* **1988**, *77*, 572.
(25) Schmider, J.; Müller, K. *J. Phys. Chem. A* **1998**, *102*, 1181.
(26) Smith, B. T.; Boyle, J. M.; Garbow, B. S.; Ikebe, Y.; Klema, V. C.; Moler, C. B. *Matrix Eigensystem Routines — EISPACK Guide*; Springer-Verlag: Berlin, 1976.

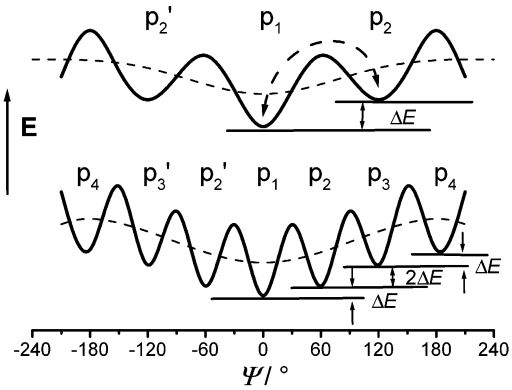

Figure 2. Potential energy scheme of a 3-site jump model (jump angle, $\Delta\Psi = 120°$; population, $p_1 \geq p_2 = p_2' = 0.5(1 - p_1)$) and a 6-site jump model (jump angle, $\Delta\Psi = 60°$; population, $p_1 \geq p_2 = p_2' \geq p_3 = p_3' \geq p_4$).

taking into account the three mirror planes of the site symmetry $\bar{3}m$ in the high-temperature phase.

The potential energy curve of the 3-site jump model is illustrated in Figure 2. The three orientations are characterized by the relative populations p_1 (0°), p_2 and p_2' (±120°), with $p_2 = p_2'$ and $p_1 + p_2 + p_2' = 1$. The ratio of the populations gives the equilibrium constant

$$K_{12} = \frac{p_2}{p_1} = \frac{(1 - p_1)}{2p_1} \tag{1}$$

for a single jump process

$$0° \overset{K_{12}}{\rightleftharpoons} \pm 120°$$

The overall potential V, a superposition of a 3-fold and a 1-fold potential, is given by

$$V(\text{3-site}) = \frac{V_1^\circ}{2}\sin\left(\Psi - \frac{\pi}{2}\right) + \frac{V_3^\circ}{2}\sin\left(3\Psi - \frac{\pi}{2}\right) \tag{2}$$

Here, the energies ΔE (Figure 2) and $V_1°$ are related via

$$\Delta E = \frac{3}{4}V_1^\circ \tag{3}$$

Likewise, the potential energy curve of the 6-site jump model (Figure 2) is described as

$$V(\text{6-site}) = \frac{V_1^\circ}{2}\sin\left(\Psi - \frac{\pi}{2}\right) + \frac{V_6^\circ}{2}\sin\left(6\Psi - \frac{\pi}{2}\right) \tag{4}$$

Again, the 6-fold potential is superimposed by a 1-fold potential. The six orientations are characterized by the relative populations p_1 (0°), p_2 and p_2' (±60°), p_3 and p_3' (±120°), and p_4 (180°), with $p_2 = p_2'$, $p_3 = p_3'$, and $p_1 + p_2 + p_2' + p_3 + p_3' + p_4 = 1$. Furthermore, the following relationships hold

$$p_1 = \frac{1}{1 + 2e^a + 2e^{3a} + e^{4a}} \tag{5}$$

$$p_2 = p_1 \times e^a$$

$$p_3 = p_1 \times e^{3a}$$

$$p_4 = p_1 \times e^{4a}$$

with $a = (-\Delta E/RT)$ and $\Delta E = {}^1/_4 V_1^\circ$ (for ΔE see Figure 2). The equilibrium constants are given by the ratios of populations

Table 1. Simulation Parameters Used During the ^{2}H NMR Data Analysis (Line Shapes, Spin−Lattice Relaxation Data)

parameter	value
quadrupolar coupling constant[a] (e^2qQ/h)	185 kHz
transformation angles[b] (deg)	
ϕ	0
θ	90
Ψ (3-site)	−120; 0; +120
(6-site)	−120; −60, 0; +60, +120, +180
residual line width [$1/(\pi T_2)$]	1000 to 4000 Hz

[a] Asymmetry parameter $\eta = 0$. [b] Euler angles ϕ, θ, Ψ relating the magnetic principal axis system and the molecular axis system (z-axis parallel to motional axis).

$$K_{12} = \frac{p_2}{p_1},\ K_{23} = \frac{p_3}{p_2},\ K_{34} = \frac{p_4}{p_3} \tag{6}$$

$$0° \overset{K_{12}}{\rightleftharpoons} \pm 60° \overset{K_{23}}{\rightleftharpoons} \pm 120° \overset{K_{34}}{\rightleftharpoons} 180°$$

This latter model which considers only nearest neighbor jumps was already used by Ripmeester during an investigation on pyridinium iodide.[2]

Quadrupole echo ^{2}H NMR line shapes were simulated for both models in the fast exchange limit by varying solely the population p_1. The additional population probabilities (3-site model, p_2; 6-site model, p_2, p_3, p_4) are related to p_1 by the 1-fold potential $V_1°$ as described above. The theoretical partially relaxed spectra simulating inversion recovery experiments were obtained by adjusting the correlation time τ_c with the known populations from the quadrupole echo spectra. The final best fit was chosen by comparison of the superimposed experimental and theoretical spectra, taking into account the overall line shapes as well as the relative amplitudes. Complementing simulation parameters are given in Table 1.

The simulation of the partially relaxed ^{2}H NMR spectra (inversion recovery experiments) was feasible with the help of

$$S(t, \tau_r) = [1 - 2 \times \exp(-\tau_r/T_{1Z})] \times S(t, QE) \tag{7}$$

Here, $S(t,\tau_r)$ and $S(t,QE)$ are the signals from the (modified) inversion recovery experiment and the quadrupole experiment in the fast exchange limit, respectively. The spin−lattice relaxation time T_{1Z} is obtained via the spectral densities J_m as given by

$$\frac{1}{T_{1Z}} = \frac{3}{16}\left(\frac{e^2qQ}{\hbar}\right)^2 \times [J_1(\omega) + 4J_2(2\omega)] \tag{8}$$

For the calculation of the spectral densities a general procedure for a N-site exchange was used, as outlined in refs 23, 25, and 27. The correlation times obey the detailed balance and are defined by

$$\frac{1}{\tau_c} = \frac{k_{ij}}{p_j} \tag{9}$$

Here, k_{ij} and p_j are the rate constant for a jump from site i to site j and the equilibrium population of site j, respectively.

DSC. A differential scanning calorimeter (Netzsch DSC-204) was used to perform heating-rate-dependent DSC measurements on $PyBF_4$-d_5 using an aluminum sample cell against an empty reference cell of the same type. The sample of $PyBF_4$-d_5 (3.9 mg) was treated according to the program

$$153\ \text{K} \xrightarrow{5\ \text{min}} 153\ \text{K} \xrightarrow{r} 273\ \text{K} \xrightarrow{5\ \text{min}} 273\ \text{K} \xrightarrow{r} 153\ \text{K}$$

(27) Wittebort, R. J.; Szabo, A. *J. Chem. Phys.* **1978**, 69, 1722.

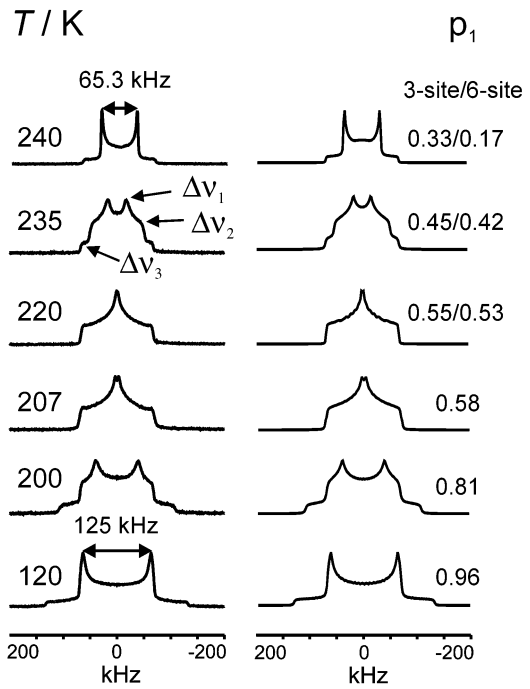

Figure 3. Temperature-dependent experimental (left) and simulated (right) ^{2}H NMR spectra, obtained via the quadrupole echo sequence. Simulated line shapes of 3-site and 6-site jump model are identical. Numbers on the right give the population p_1.

with r giving the heating rate of 2 K min^{-1}, 5 K min^{-1}, and 10 K min^{-1}. The program cycle was repeated twice. The molar heat capacity c_p was obtained using the heat flux $\dot{Q} = dQ/dt$ per sample mass m, the heating rate $r = \mathrm{d}T/\mathrm{d}t$, and the molar mass $M = m/n$:

$$c_p = \dot{Q} \times M/(r \times m) = (1/n) \times dQ/dT \qquad (10)$$

3. Results

^{2}H NMR Spectra. Representative ^{2}H NMR spectra of the powder sample covering all three phases are shown in Figure 3. It is quite obvious that both phase transitions have a strong impact on the corresponding line shapes. In general, the distinct features (i.e., sharp singularities) of these ^{2}H NMR spectra imply the presence of motions that are in the fast exchange limit on the NMR time scale, as further verified by additional T_2 experiments. In the high-temperature phase ($T >$ 238.7 K) axially symmetric ^{2}H NMR line shapes are detected. The observed splitting between the perpendicular singularities of $\Delta\nu_\perp = 65.3$ kHz is independent of temperature and considerably reduced as compared to the "rigid limit" value. These observations clearly indicate the presence of a highly symmetric and efficient motional process.

Cooling the sample below the phase transition at 238.7 K results in typical nonaxially symmetric ^{2}H NMR line shapes. In the intermediate phase the overall ^{2}H NMR pattern is found to vary continuously with the actual sample temperature. Again, the experimental ^{2}H NMR line shapes can be understood on the basis of a fast motional process which now must be of lower symmetry.

The second (low temperature) phase transition at 204 K is reflected in the ^{2}H NMR line shapes by a sudden change of the spectral splittings. Upon further cooling to 120 K an almost "rigid limit" powder pattern is observed. Now, the experimental splitting between the perpendicular singularities is given by 125 kHz, a value that is expected for an almost completely immobile pyridinium cation. The experimental splittings between the spectral singularities, as derived from the variable temperature ^{2}H NMR line shapes, are summarized in Table 2.

Table 2. Experimental Splittings between Singularities in the ^{2}H NMR Spectra[a] (See Figure 3)

T/K	$\Delta\nu_1$/kHz	$\Delta\nu_3$/kHz	T/K	$\Delta\nu_1$/kHz	$\Delta\nu_3$/kHz
120	125	265	220	1.98	127
140	123	261	230	15.8	111
160	121	254	235	31.7	91.1
180	109	242	237	47.5	83.2
200	79.2	230	238[b]	51.5	79.2
203	63.4	194	238[c]	65.3	79.2
204[b]	55.5	190	240	65.3	65.3
205[b]	51.5	186	245	65.3	65.3
204[c]	7.92	190	250	65.3	65.3
205[c]	7.92	186	270	65.3	65.3
207	5.94	143	290	65.3	65.3
210	3.96	139			

[a] $\Delta\nu_2$ = 131 kHz = const. [b] 1st spectral component. [c] 2nd spectral component, see text.

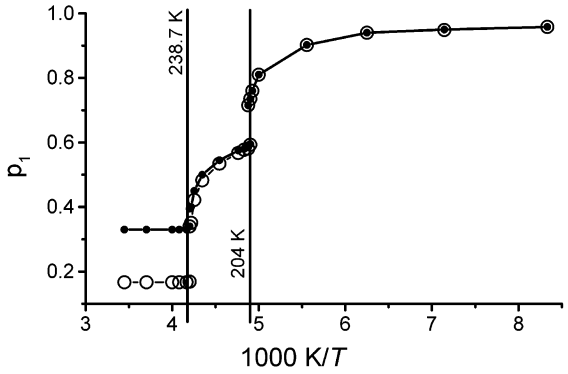

Figure 4. Population p_1 of the lowest energy orientation (solid symbols, 3-site model; open symbols, 6-site model). Phase transitions are indicated with vertical solid lines (literature values, ref 11).

The theoretical ^{2}H NMR spectra, given in Figure 3, were obtained assuming a 3-site jump process and a motional symmetry axis that is parallel to the pseudo $C6$ axis of the cation. A comparison of the experimental and the theoretical line shapes shows that the chosen simulation model is appropriate to describe the experimental spectra very well. In the high-temperature phase we find equally populated sites ($p_1 = p_2 = 0.33$), whereas below 238.7 K, upon cooling, p_1 increases at the expense of populations p_2 and p_2'. The temperature dependence of the population p_1 is given in Figure 4. Again, distinct discontinuities are observed at the phase transitions.

As expected, on the basis of the 6-site jump model an equally good reproduction of the experimental spectra could be achieved as for the 3-site jump case. The temperature dependence of the population p_1 (also given in Figure 4) is identical to that of the 3-site jump case in the low-temperature phase, and almost identical in the intermediate-temperature phase. In the high-temperature phase equally populated sites are found (6-fold jumps, $p_1 = 0.167$; 3-fold jumps, $p_1 = 0.33$).

Spin Lattice Relaxation Experiments. Representative experimental partially relaxed ^{2}H NMR spectra

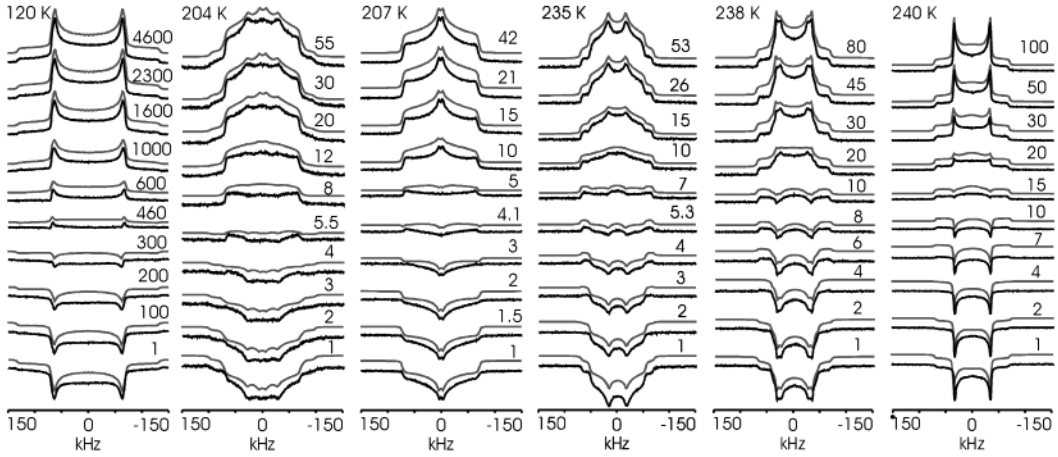

Figure 5. Experimental (black) and simulated (gray) partially relaxed ^{2}H NMR spectra (inversion recovery experiment) at selected temperatures. Simulations are slightly offset to facilitate comparison and are identical for the 3-site and 6-site jump models. Numbers on the right refer to the relaxation delay times τ_r in ms.

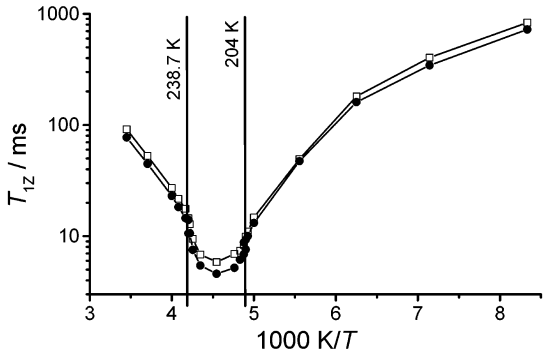

Figure 6. Experimental (open squares) and simulated (solid circles) T_{1Z} relaxation data (simulated data are identical for both simulation models). Phase transitions are indicated by vertical solid lines.

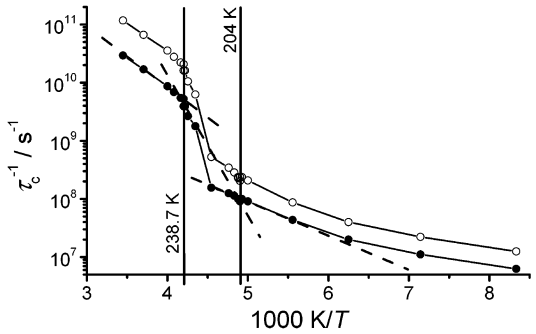

Figure 7. Arrhenius plot of the correlation times derived from the 3-site jump model (solid symbols) and the 6-site jump model (open symbols). Phase transitions are indicated by vertical solid lines. Dashed lines represent the slopes used in case of the 3-site jump model to derive the activation energies $E_A^{\#}$.

(inversion recovery experiments) are displayed in Figure 5. T_{1Z} values (overall powder values) determined from the experimental free induction decays are plotted in Figure 6. They build up a very characteristic curve covering a T_{1Z} range from 5 to 800 ms. The T_{1Z} minimum, at which the motion of the cations occurs at about the Larmor frequency of 46.07 MHz, is found at $T = 220$ K.

Again, the two phase transitions have an impact on the T_{1Z} data, as reflected by a change of the slope of the T_{1Z} curve. Furthermore, in the low-temperature phase the slope of the T_{1Z} curve is not constant. Rather, the T_{1Z} curve levels off toward lower temperatures. It should be noted that saturation effects can be completely ruled out and are not responsible for this latter observation.

In general, the simulated line shapes, given in Figure 5, provide a very good reproduction of their experimental counterparts. The theoretical partially relaxed ^{2}H NMR spectra obtained on the basis of the aforementioned 3-site jump model are identical to those obtained from the 6-site jump model. The same holds for the theoretical T_{1Z} values which are plotted in Figure 6. The largest deviations are found close to the T_{1Z} minimum, where the theoretical values are somewhat lower than the experimental ones. The correlation times τ_c for both models, derived from the analysis of the partially relaxed ^{2}H NMR spectra, are displayed in Figure 7.

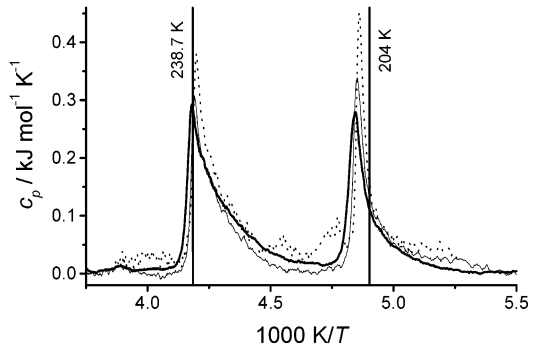

Figure 8. Baseline-corrected DSC measurements of $PyBF_4$-d_5 at 2 K min^{-1} (dotted line), 5 K min^{-1} (solid line), and 10 K min^{-1} (bold solid line) (all heating curves). Phase transitions are indicated by vertical solid lines (literature values, ref 11).

DSC Measurements. Heating-rate-dependent DSC measurements were performed on $PyBF_4$-d_5 (Figure 8). The extrapolated phase-transition temperature from the heating and the cooling curves agreed within the experimental error of ±0.3 K with each other so that no supercooling was detected; but the low-temperature phase transition was found to occur at 205 K instead of the reported value of 204 K.[11,28] For comparison, analo-

(28) Szafraniak, I.; Czarnecki, P.; Mayr, P. U. *J. Phys.: Condens. Matter* **2000**, *12*, 643.

gous experiments with perdeuterated pyridinium perchlorate, where it is generally agreed that both phase transitions are of first order,[29] revealed a supercooling of 1.5 K for the low-temperature transition and 4.4 K for the high-temperature transition.

4. Discussion

^{2}H NMR Spectroscopy. The experimental ^{2}H NMR spectra of $PyBF_4$-d_5 are found to be in the fast motional limit which is true for the whole temperature range covered in the present study. In particular this also holds for the low-temperature phase where correlation times larger than 10^{-8} s are observed. Here, the population p_1 is close to unity; the quadrupolar interaction is therefore only slightly modulated by the underlying motional process of the cations, as shown also by independent line shape simulations. The assumption of the fast motional limit is therefore justified.

Furthermore, all deuterium atoms in the pyridinium molecule must be equivalent, as the experimental ^{2}H NMR spectra exhibit a single powder pattern. A rotation around the molecular *C*2 axis or pseudo *C*2 axis in the pyridinium plane can be excluded, since in these cases the deuterium atoms would be nonequivalent and would give rise to different motionally averaged sub-spectra. The axially symmetric ^{2}H NMR line shapes in the high-temperature phase can be understood on the basis of a single molecular process. Hence, a fast rotation (3-fold or 6-fold jumps between equally populated sites) about the pseudo *C*6 axis — the molecular plane normal — takes place which coincides with the [111] crystal axis (Figure 1). It should be mentioned that an independent proof for our motional model was provided by the ^{2}H NMR spectra of N-deuterated $PyBF_4$ (spectra not shown), as they are identical to those discussed here for $PyBF_4$-d_5. Likewise, the comparison with a previous ^{2}H NMR study on perdeuterated benzene-d_6 in the solid plastic phase,[30] for which the same unhindered motion around the molecular *C*6 axis was derived, demonstrates a close resemblance with the present data on $PyBF_4$ in the high-temperature phase.

The nonaxially symmetric ^{2}H NMR spectra in the intermediate and low temperature phases (T < 238.4 K) can be attributed to nondegenerate rotational jumps (nonequally populated jump sites). The observed spectral changes upon sample cooling can be rationalized by the increase in population p_1. The most distinct changes of the cation motion take place around the phase transitions. The ^{2}H NMR spectra at 204 K, 205 K, and at 238 K, i.e., at the calorimetric phase transitions (see also Figure 5), are the only examples with two pairs of sub-spectra (Table 2) due to two coexisting phases. In general the phase transitions are accompanied by a change of crystal symmetry, as also reflected in the ^{2}H NMR data. Thus, the high-temperature phase transition (238.7 K) gives rise to a slight compression of the [111] axis which limits the space between the individual cation layers and hinders the rotational motion of the pyridium ions.

The very good reproduction of the experimental data from both the quadrupole echo and the inversion recovery experiments demonstrates that the 3-site jump model, as well as the 6-site jump model, can fully describe the cation reorientational motion in $PyBF_4$-d_5. Attempts with a simple 2-site jump model (equally populated sites, varying jump angle) provided a good fit of the (fully relaxed) quadrupole echo line shapes as well, but failed for the description of the partially relaxed spectra from the inversion recovery experiments. So far, more sophisticated motional models — such as combinations of jump motions with oscillatory motions, distributions of correlation times, etc. — were not further tested. It might well be that such models provide an even better fit of the experimental data in the vicinity of the T_{1Z} minimum (see above).

The theoretical partially relaxed ^{2}H NMR line shapes (inversion recovery experiments) obtained from the 3-site jump model yield the correlation times τ_c covering a range from 2×10^{-7} s to 3×10^{-11} s. The rate constants $k = 1/\tau_c$, which are displayed in Figure 7, give the number of all individual jumps per unit time.[31,32] For the 6-site jump model the rate constant plot shows an identical shape, but the individual values are all shifted upward (range of correlation times τ_c, 1×10^{-7} s to 1×10^{-11} s).

In general, the rate constants in the various phases follow an Arrhenius behavior for both models. In the intermediate phase a point is found outside the regression line, which stems from the discrepancy between the experimental and theoretical T_{1Z} data, as mentioned earlier. Likewise, in the low-temperature phase the rate constants at 120 and 140 K do not follow the Arrhenius behavior, which is a direct consequence of the experimental T_{1Z} data (see above). This latter observation might be traced back to the presence of an additional mechanism that contributes to ^{2}H spin relaxation at low temperatures, as, for example, by the motion of the tetrafluoroborate anion. Forthcoming ^{11}B NMR experiments should provide additional information on this topic.

The activation energies ($E_A^{\#}$), derived from the slopes in the Arrhenius plot in Figure 7 for the 3-site jump model, are 19.3, 46.4, and 10.0 kJ mol^{-1} in the high-, intermediate-, and low-temperature phases, respectively. In the case of the 6-site model they amount to 19.1, 54.0, and 11.2 kJ mol^{-1}, respectively. Very similar values of 17.6 kJ mol^{-1} for pyridinium iodide and 17.4 kJ mol^{-1} for pyridinium tetrafluoroborate were reported by Ripmeester[3] and Wasicki et al.[33], respectively. Likewise, the high-temperature values are also comparable to that of *C*6 rotation in pure solid benzene (16.5 kJ mol^{-1}), as reported by Ok et al.[30]

The frequency factors (A) for the 3-site jump model amount to 8.9×10^{13} s^{-1}, 6.1×10^{19} s^{-1}, and 3.7×10^{10} s^{-1}, with the intermediate value once more being unexpectedly high. The corresponding values in the 6-site jump case are 3.3×10^{14} s^{-1}, 1.2×10^{22} s^{-1}, and 1.8×10^{11} s^{-1}. Obviously, the activation energy and the frequency factor are strongly correlated.

(29) Wasicki, J.; Lewicki, S.; Czarnecki, P.; Ecolivet, C.; Pajak, Z. *Mol. Phys.* **2000**, *98* (10), 643.
(30) Ok, J. H.; Vold, R. R.; Vold, R. L.; Etter, M. C. *J. Phys. Chem.* **1989**, *93*, 7618.
(31) Bovey, F. A.; Anderson, E. W.; Hood, F. P.; Kornegay, R. L. *J. Chem. Phys.* **1964**, *40*, 3099.
(32) Anderson, J. E. *J. Magn. Res.* **1973**, *11*, 398.
(33) Wasicki, J.; Pajak, Z.; Kozak, A. *Z. Naturforsch.* **1990**, *45a*, 33.

This behavior, and the unreasonably high parameters in the intermediate phase, point to the presence of a composite process. If, for an alternative analysis, the high-temperature frequency factor is assumed to remain valid also for the intermediate phase, the experimental correlation times can be matched also with a stepwise increase of the activation energy from 19 to 24 kJ mol^{-1} over the intermediate phase. It reflects the way ΔE (and thus $V_1°$) is built up when the high-temperature symmetry is broken and the pyridinium ions experience a preferential orientation in the electric field that is provided by the macroscopic polarization.

Ferroelectric Polarization. The polarization is defined as the average electric dipole moment per unit volume. The orientational contribution is calculated from the temperature-dependent population of the cation orientations in the case of the 3-site jump model

$$pol(\text{3-site}) = p_1 - 2p_2\cos(60°) = 1.5p_1 - 0.5 \quad (12a)$$

and in the case of the 6-site jump model

$$pol(\text{6-site}) = p_1 - 2p_2\cos(60°) - 2p_3\cos(60°) - p_4 = p_1 + p_2 - p_3 - p_4 \quad (12b)$$

if the molecular electric dipole moment of the cation is known. Therefore, quantum chemical calculations using Gaussian98 based on B3LYP functionals with various basis sets were undertaken. They revealed that the dipole moment is nearly basis set independent. It amounts to 1.876±0.006 D for the simpler basis sets (6-31G*, 6-31G**, 6-311G*) and 1.810±0.004 D for the more sophisticated (6-311++G(2df,2pd)) basis set. The use of augmented basis sets did not introduce any further change. Calculations for the pyridine molecule showed that the results for the simpler basis sets are very close to the literature value. Therefore the first value (1.876 D) was chosen for further analysis. The dipole moment is situated in the molecular plane of the pyridinium cation and points at the nitrogen atom. The center of the cation charge is, in general, not expected to coincide with the cation rotation axis. When the orientational order increases, this would lead to an additional contribution to polarization of the displacement type of positive and negative charge sublattices, without actually displacing the ion center of masses. To check for this effect, the dipole moment was also calculated for a pyridinium cation located in an anion matrix. This matrix consisted of eight point charges (−0.125 |e| each), arranged around the cation according to the low-temperature unit cell structure. Rotation of the cation shows that the effective dipole moment is indeed slightly orientation dependent, but the variations are too small (<2%) to show a significant effect on the polarization.

The population-averaged dipole moment per cation, as determined from the NMR data, times the number of cations per unit volume, then gives the orientational contribution to the absolute polarization. The curves for both models are shown in Figure 9 along with the macroscopic polarization reported from pyroeffect measurements by Czarnecki et al. on a $PyBF_4$ single domain single crystal.[11] Because of identical population of all orientations there is no polarization in the high-temperature phase. In the intermediate phase the values

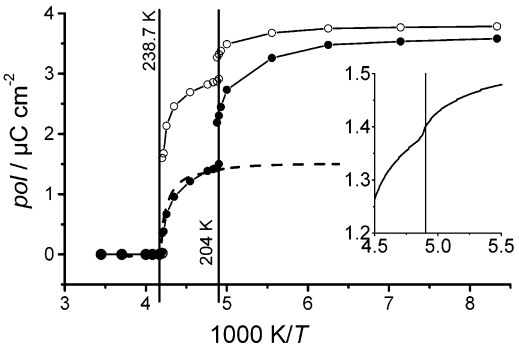

Figure 9. Polarization derived from NMR populations using equations 2a (3-site, solid symbols) and 2b (6-site, open symbols), and spontaneous polarization obtained from pyroeffect measurements (dashed line) by Czarnecki et al.[11]. The inset shows an expansion of the macroscopic polarization around the low-temperature phase transition.

rise to about 1.4 μC cm^{-2} at 204 K for the data from both the analysis of the NMR data (3-fold jump model) and the pyroeffect measurements, and the two curves agree almost within error. However, in the low-temperature regime the polarization from the pyroeffect shows only a slight further increase (see inset of Figure 9), whereas the values derived from NMR data (3-site) rise to 3.6 μC cm^{-2} at 120 K, which is more than double the value at 204 K. In the case of the 6-site jump model a quite different behavior is observed. The polarization rises already at the high-temperature transition to a value of 2.9 μC cm^{-2}, that is 60% of the total value of 3.8 μC cm^{-2} which is reached at 120 K.

The NMR data represent only the cation rotational order. Therefore, the good agreement between the two curves in the intermediate temperature regime, as found for the case of the 3-site jump model, implies that here the ordering of the cations is the only mechanism contributing to the macroscopic polarization. The obvious discrepancy between the two curves in the low temperature regime (T < 204 K) reveals that an additional mechanism with an opposite effect contributes to the polarization. The polarizability of the pyridinium cations is too small to account for this, and moreover it should operate also in the intermediate temperature phase. It seems that only the classical ferroelectric mechanism, a translational displacement of cation versus anion sublattice, is left as a reasonable origin of the discrepancy. Obviously, in the low-temperature phase below 204 K, the lattice can no longer withstand the force imposed by the increasing electric field of the ordering molecular dipoles, so that the system relaxes by an increasing slip of the two sublattices against each other, thereby spring-loading the crystal. The full difference of 2.1 μC cm^{-2} between NMR and pyroeffect measurements at 120 K is equivalent to a dipole moment of 1.11 D, which corresponds to a displacement of 0.23 Å of the anion relative to the cation sublattice.

Likewise, the total difference in polarization in the low-temperature phase between the data from the analysis with the 6-site jump model and from the pyroeffect data is only slightly higher than that discussed above for the 3-site jump model. The value of 2.3 μC cm^{-2} in the low-temperature limit corresponds to a displacement of 0.25 Å. In the intermediate-

temperature regime, the polarization curve obtained from the 6-site jump model is not identical to the pyroeffect data, but it shows the same trend. That is why we conclude that the total displacement in the case of the 6-site jump model is generated in a two-step process, 0.15 Å of displacement already builds up in the intermediate-temperature phase and the additional 0.1 Å builds up in the low-temperature phase. A new structure determination with a single-domain single crystal at low temperature is called for to discriminate between the two different models.

Critical Behavior. Fitting the NMR polarization curve obtained with the 3-site jump model in the intermediate phase according to Landau's theory to a function

$$pol = pol_0[1 - (T/T_n)]^c \quad (13)$$

reproduces the data very well and results in a critical exponent c of 0.286 (T_n = 237.30 K, pol_0 = 2.356 μC cm^{-2}). This is close to the value of 0.25 that corresponds to a tricritical transition.[34] It indicates a behavior at the borderline between a first- (c undefined) and a second-order (c = 0.5) transition. Fitting the NMR data obtained from the 6-site jump model yields a critical exponent c of 0.156 (T_n = 238.00 K, pol_0 = 3.998 μC cm^{-2}) which is much closer to a first-order than to a second-order transition. The macroscopic polarization data of Czarnecki et al.[11] is somewhat rounded off just below the high-temperature transition and was therefore not fitted. The determination of a critical exponent around the low-temperature transition in the NMR curves of both models was not possible because of the uncertainty of how to treat the background from the intermediate phase.

Thermodynamic Properties. For the analysis of the thermal properties we start from the standard relation between the enthalpy H and the internal energy U

$$dH = dU + pdV + Vdp \quad (14)$$

and note that

$$dU = dQ + dW_{vol} + dW_{fe} = dQ - pdV + dW_{fe} \quad (15)$$

where the unconventional term W_{fe} denotes the ferroelectric work in the crystal lattice (see below). Under condition of constant pressure we obtain

$$\Delta H_{(T_1 \rightarrow T_2)} = Q_p + W_{fe} = \int_{T_1}^{T_2} c_p dT + \int_{T_1}^{T_2} c_{fe} dT \quad (16)$$

where c_{fe} is a formal analogue of the heat capacity which is not detectable calorimetrically. As the temperature is lowered below 238.7 K, the energy of the system decreases by alignment of the molecular dipoles. A fraction of this energy Q_p is released as heat (mostly the one that relates to de-excitation of lattice vibrational modes; it can be measured in a calorimeter), while the other fraction W_{fe} is stored in the capacitance of the polarizing domains, and below 204 K mainly as potential energy of the spring-loaded domains. We will now derive from our NMR data those thermodynamic properties of the system which refer to the orientational order of the cations. In analogy to the van't Hoff relation for the temperature dependence of a chemical equilibrium we write for the fractional enthalpy change ΔH_n between two successive temperature points n and $n + 1$ in the case of the 3-site jump model

$$\Delta H_n = -f \times R \frac{\Delta(\ln K)}{\Delta(1/T)} \quad (17)$$

where $f = p_{1,n} - p_{1,n+1}$ is the fraction of molecules changing from p_1 to p_2 or p_2' within this temperature interval, and $K = K_{12}$ is the equilibrium constant, as defined earlier. ΔH_n represents the difference in activation energies for a jump process out of and into the highest populated orientation. Considering the 6-site jump model ΔH_n consists of the different contributions of the individual jump processes ($\Delta H_n = \Delta H_{12} + \Delta H_{23} + \Delta H_{34}$) taking into account the individual equilibrium constants K_{12}, K_{23}, and K_{34} (see above). The individual factors f are given by $f_{12} = p_{1,n} - p_{1,n+1}$, $f_{23} = f_{12} - 2(p_{2,n+1} - p_{2,n})$, and $f_{34} = p_{4,n+1} - p_{4,n}$, and give the individual fraction of molecules changing from 0° to ±60°, from ±60° to ±120°, and from ±120° to 180°, respectively.

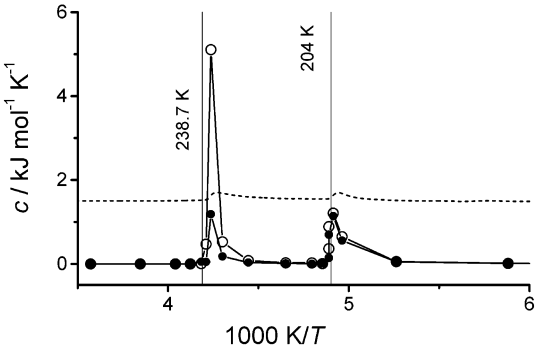

Figure 10. Heat capacity, $c = c_p + c_{fe}$, calculated from NMR populations (solid symbols, 3-site jump model; open symbols, 6-site jump model; for populations see also Figure 4) and c_p from DSC measurements (dashed line, 10 K min^{-1}, see also Figure 8; DSC data are shifted upward by 1.5 kJ mol^1 K^{-1} to permit comparison).

From ΔH_n we obtain the NMR-derived "heat capacities" $c = \Delta H_n/\Delta T_n = c_p + c_{fe}$, at intermediate temperatures, $T = (T_n + T_{n+1})/2$ for both simulation models. They are shown in Figure 10 together with the baseline-corrected conventional calorimetric data. Deviations of the phase-transition temperatures from the literature values are due to the mean temperature values used in the analysis of the NMR data in combination with a minimum temperature difference of only 1 K. Clearly, an analogous behavior is observed, but the NMR-derived spikes are much sharper than the macroscopic ones, leading to higher values at the phase-transition temperatures. Comparing the two simulation models, the values are identical at the low-temperature transition, but much higher for the 6-site jump model at the high-temperature transition. More meaningful perhaps are the integrated enthalpy changes, $\Sigma\Delta H_n$ (Figure 11). In the intermediate temperature range the NMR-derived enthalpy change related to the 3-site jump model amounts to 4.0 kJ mol^{-1}, which is only slightly more than the DSC value of 3.2(2) kJ mol^{-1}. The difference

(34) Gieβelmann, F. In *Selforganization in Chiral Liquid Crystals;* Kuczynski, W.; Scientific Publishers OWN: Poznan, 1997; p 7.

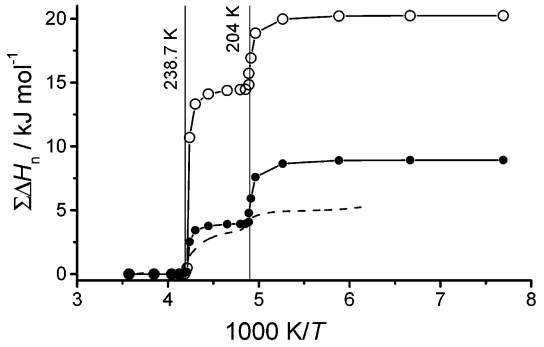

Figure 11. Total change of enthalpy from NMR data (solid symbols, 3-site jump model; open symbols, 6-site jump model) and from DSC measurements (10 K min^{-1}) (dashed line).

Table 3. Kinetic, Thermodynamic, and Ferroelectric Properties Derived in the Present Work

	model	lt[a]	it[b]	ht[c]
activation energy[d] $E_A^{\#}$	3-site	10.0	46.4	19.3
(kJ mol^{-1})	6-site	11.2	54.0	19.1
frequency factor[d]	3-site	3.7×10^{10}	6.1×10^{19}	8.9×10^{13}
(A/ s^{-1})	6-site	1.8×10^{11}	1.2×10^{22}	3.3×10^{14}
polarization difference	3-site[d]	2.2	1.4	0.0
$\Delta pol/\mu C\ cm^{-2}$	6-site [d]	0.9	2.9	0.0
	pyro[e]	0.1	1.4	0.0
enthalpy change	3-site[d]	5.0	4.0	0.0
$\Sigma\Delta H_n$/ kJ mol^{-1}	6-site [d]	5.5	15	0.0
	DSC	1.6(3)	3.2(2)	0.0

[a] Low-temperature phase. [b] Intermediate-temperature phase. [c] High-temperature phase. [d] NMR. [e] Pyroeffect measurements by Czarnecki et al.[11]

is attributed to the energy that is stored in the capacitance of the polarized domains. However, the accuracy of the DSC data is limited so that this point is not further discussed. More dramatic is the situation in the low-temperature phase. From NMR (3-fold jumps) we derive an enthalpy change between 120 and 204 K of 5.0 kJ mol^{-1}, while only 1.6(3) kJ mol^{-1} were measured calorimetrically. This means that most of the energy is stored as strain energy due to the relative displacement of the two sublattices. In the case of the 6-site jump model this looks quite different. In the intermediate temperature range the change of enthalpy already amounts to 15 kJ mol^{-1} which is nearly five times more than that derived by DSC, and nearly four times more than that determined with the 3-site jump model. For the low-temperature regime an additional change of enthalpy of 5.5 kJ mol^{-1} is observed. This is comparable to that found in the 3-site jump case, but again much higher than that found by DSC. All results are listed in Table 3.

The difference between the NMR and DSC enthalpy changes, $\Delta E_x = \sum\Delta H_n(\mathrm{DSC}) - \sum\Delta H_n(\mathrm{NMR}) = {}^1/_2 k \times x^2$ (see Figure 11), maps the potential along the displacement coordinate x that is calculated from the polarization (see discussion of Figure 9). On this basis we estimate the force constant k and the lattice vibrational frequency along this coordinate for the 3-site jump model and obtain a frequency of 102 cm^{-1} (at 120 K) up to 170 cm^{-1} in the low-temperature phase. These values are comparable to those of the direct Raman spectroscopic determination by Ecolivet et al. (145 cm^{-1}).[35] The 6-site jump model yields frequencies of 181 cm^{-1} up to 200 cm^{-1} in the low-temperature regime. This is almost constant as expected for a harmonic potential; but the values are higher than those found by Ecolivet et al. In the intermediate-temperature regime the frequency amounts to 230 cm^{-1} up to 280 cm^{-1} for the 6-site jump model.

In contrast to the enthalpies, the free energies ΔE are obtained directly from the simulations according to relations (1) and (6). The temperature dependence of the free energies is almost identical for both models and the overall characteristic resembles the p_1 curve shown in Figure 4. Below the high-temperature transition ΔE rises up to 2.0 kJ mol^{-1} at 204 K, and to a maximum value of 4.6 kJ mol^{-1} within the low-temperature phase.

5. Conclusion

In the present work $PyBF_4$-d_5 was studied by ^{2}H NMR spectroscopy between 120 and 290 K. The experimental ^{2}H NMR data (line shapes, spin−lattice relaxation times) can be completely described by a single molecular process of the pyridinium ions, namely a rotation around the pseudo $C6$ axis. In the high-temperature phase above 238.7 K, $PyBF_4$-d_5 exhibits a fast rotation (3-fold or 6-fold jumps) between equally populated sites, with similar activation parameters as reported earlier for the rotation of pyridinium ions in $PyBF_4$ and in pyridinium iodide or even benzene in the solid state. In the intermediate- and low-temperature phases the motion becomes progressively impeded resulting in nearly static cations (on the NMR time scale) at 120 K. Here, a nondegenerate 3-site jump model as well as a nondegenerate 6-site jump model can describe both the experimental ^{2}H NMR (quadrupole echo) spectra and the partially relaxed line shapes and T_{1Z} data from the inversion recovery experiments. On the basis of both models the analysis of the variable temperature ^{2}H NMR data reveals distinct changes of the pyridinium properties (correlation times, population of jump sites) in the vicinity of the two solid−solid phase transitions.

A simple 2-site jump model (accounting for oscillatory motions) can be ruled out, as it failed for the description of the T_{1Z} data and partially relaxed spectra. It is important to note that the present NMR data can be described adequately by both the 3-fold and the 6-fold jump models. It is therefore not possible to make a final statement about the correct model for the cation motion in the system examined here. The 3-fold rotation-inversion axis in the high-temperature phase is compatible with a 6-fold jump process, which is also plausible based on the near 6-fold symmetry of the pyridinium ion. Upon passing both solid−solid phase transitions toward lower temperature the symmetry is lowered. However, the structural change appears to be only marginal, suggesting that the 6-fold jump model may still be a better approximation and probably more plausible than the simpler 3-fold jump model.

Hanaya et al. proposed that ferroelectricity originates from the orientational ordering of the tetrafluoroborate anions.[13] Although it is plausible that the anion disorder contributes significantly to heat capacity and entropy, it cannot contribute to ferroelectricity unless the anion is significantly distorted from tetrahedral symmetry. We postulate that in addition to cation ordering, the clas-

(35) Ecolivet, C.; Czarnecki, P.; Wasicki, J.; Beaufils, S.; Girard, A.; Bobrowicz-Sarga, L. *J. Phys.: Condens. Matter* **2001**, *13*, 6563.

sical ferroelectric mechanism contributes with an opposite effect on polarization, as the polarization obtained from the NMR data is much larger than the macroscopic one. An anion versus cation sublattice displacement of around 0.23−0.25 Å can account for the missing polarization.

Enthalpy data derived from the NMR measurements reveal that for the low-temperature phase only a fraction of the energy required to induce orientational disorder on heating is actually heat, the major fraction is released potential energy that arises from relaxation of the relative displacements of the anion vs the cation sublattices. The same holds in the intermediate-temperature regime for the 6-site jump model (but for the 3-site jump model the NMR-derived enthalpy change agrees nearly with the calorimetric determination). An estimate of the vibrational frequency in the low-temperature phase yields values which are comparable with the experimental ones, and this supports our interpretation on the basis of the sublattice displacement model.

Regarding the question of the order of the two phase transitions we summarize as follows. Typical criteria for first order are supercooling and phase coexistence. Other than for $PyClO_4$ (which has almost the same lattice structure as $PyBF_4$ and two ferroelectric phases as well, but where there is no doubt that both transitions are of first order[28]) we find no evidence of supercooling when we extrapolate to zero heating/cooling rates. Nevertheless, the spectra at 204, 205, and 238 K reveal the contribution of two spectra with slightly different splittings, but it is not excluded that this could be due to temperature inhomogeneity. ALC-μSR measurements showed a steplike change of the line widths for $PyClO_4$ but a smooth behavior for $PyBF_4$ at the higher temperature transition.[36] The specific heat changes show very broad tails on the low-temperature side of each transition as it is typical for order−disorder transitions. The two features sharpen only slightly upon reduction of the heating rate (Figure 8). The ferroelectric polarization curves are likewise discontinuous, but with a broad onset; only the high-temperature transition in the 3-site jump model may show a continuous behavior. The high-temperature transition in the 3-site jump model fits very well critical behavior with a close to tricritical exponent, pointing to a borderline case between first and second order, whereas the critical exponent determined for the 6-site jump process is closer to a first-order transition. We point out that both ferroelectric polarization mechanisms, the cation orientational order and the sublattice relative displacement, have a continuous onset and satisfy the Ehrenfest requirement for second-order phase transitions. Although our results tend to support Czarnecki's interpretation of the phase transitions[29] they are clearly at variance with the work by Hanaya et al., who attributed ferroelectricity to orientational order of the tetrafluoroborate anions.[13] It would be interesting to see the results of an up-to-date structure determination of the low-temperature phase and the result of analogous NMR experiments with $PyClO_4$.

Acknowledgment. We thank Gerald Fritsch for support during the NMR measurements. We are grateful to Piotr Czarnecki for helpful discussion, and we acknowledge the support of Ilaria Ciofini and Georg Hübner concerning the quantum chemical calculations. The DFG (Deutsche Forschungsgemeinschaft) is thanked for financial support through the Graduate College 448 on "Modern Methods of Magnetic Resonance in Materials Science" at the University of Stuttgart.

CM021224E

(36) Beck, B.; Roduner, E.; Dilger, H.; Czarnecki, P.; Fleming, D. G.; Reid, I. D.; Rhodes, Ch. J. *Physica B* **2000**, *289−290*, 607.